Biophysical Modeling of a *Drosophila* Photoreceptor

Zhuoyi Song[1,2], Daniel Coca[1], Stephen Billings[1], Marten Postma[3], Roger C. Hardie[3], and Mikko Juusola[2]

[1] Department of Automatic Control and Systems Engineering, University of Sheffield, Mappin Street, Sheffield, S1 3JD, UK
[2] Department of Biomedical Science, University of Sheffield, Western Bank, S10 2TN, Sheffield, UK
[3] Department of Physiology, Development and Neuroscience, Cambridge University, Downing Street, Cambridge, CB2 3DY, UK
{zhuoyi.song,d.coca,S.Billings}@sheffield.ac.uk,
m.postma@uva.nl, rch14@cam.ac.uk, m.juusola@sheffield.ac.uk
http://www.shef.ac.uk/acse/spcs

Abstract. It remains unclear how visual information is co-processed by different layers of neurons in the retina. In particular, relatively little is known how retina translates vast environmental light changes into neural responses of limited range. We began examining this question in a bottom-up way in a relatively simple fly eye. To gain understanding of how complex bio-molecular interactions govern the conversion of light input into voltage output (phototransduction), we are building a biophysical model of the *Drosophila* R1-R6 photoreceptor. Our model, which relates molecular dynamics of the underlying biochemical reactions to external light input, attempts to capture the molecular dynamics of phototransduction gain control in a quantitative way.

Keywords: Biophysical model, *Drosophila* photoreceptor, phototransduction cascade, Gillespie algorithm, Hodgkin-Huxley model.

1 Introduction

There have been many approaches to model fly photoreceptors [17,15,14,13]. van Hateren produced a linear-nonlinear cascade model to compare phototransduction in blowfly photoreceptors to that of primate cones [17]; Pumir and his co-workers produced a biophysical model of fly phototransduction cascade [15]; Váhásőrinki et al. developed a Hodgkin-Huxley model, which relates Light Induced Current (LIC) to voltage response, to study the effect of voltage-gated potassium channels on visual information processing [10]. There are also models for intracellular calcium dynamics, such as the diffusion model introduced by Postma et al. [14] and the calcium homeostasis model by Oberwinkler [11].

To begin to investigate how a network of photoreceptors and interneurons, whose responses are shaped together through feed-forward and feedback synapses,

C.S. Leung, M. Lee, and J.H. Chan (Eds.): ICONIP 2009, Part I, LNCS 5863, pp. 57–71, 2009.

co-process visual information, we developed a new biophysical model for *Drosophila* photoreceptor, which will form the input stage for a more complex network model that will be developed in the near future. Our model describes both photo-sensitive and photo-insensitive membranes of the photoreceptor. The photo-sensitive part of the model consists of linear and nonlinear differential equations describing biochemical reactions involved in phototransduction cascade. The photo-insensitive membrane is represented by an electrical circuit model based on Hodgkin-Huxley formalism. The complete model can predict quite well macroscopic current and voltage responses to varying light impulses (patch-clamp data from whole cell recordings).

2 Structure of *Drosophila* Photoreceptor

The compound eye of *Drosophila* (Fig. 1A) contains 776 ommatidia, stereotypical processing units that focus the light energy by a corneal lens onto the rhabdom, the light-sensitive parts of the photoreceptors underneath. Inside of each ommatidium, the outer photoreceptors (R1-R6) are arranged in a ring, surrounding the inner R7 and R8 photoreceptors, which are stacked on top of each other in the center. This gives ommatidia a characteristic pattern of 7 disks when viewed from the top or in cross-section (Fig. 1D). R1-R8 are arranged around a central space, intraommatidial cavity. Fig. 1E shows that *Drosophila* photoreceptors are thin elongated cells, 100 μm in length (excluding axon) and $5-6$ μm in diameter. Their plasma membranes divide into photo-sensitive (rhabdomere) and

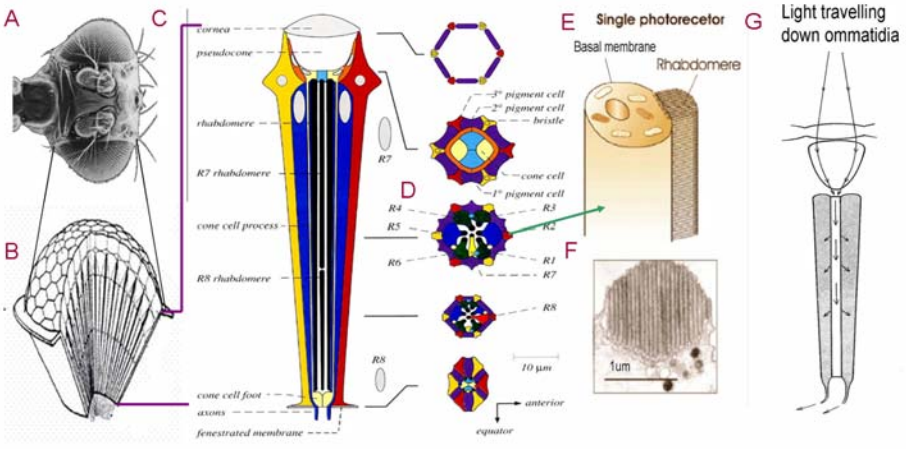

Fig. 1. Anatomy of *Drosophila* eye. (A) The head. (B) Slice of a compound eye. (C) Vertical section of ommatidium. (D) Cross section of ommatidium. (E) Schematic single photoreceptor. (F) Cross section of Rhabdomere. (G) Light pathway. (C) and (D) are modified from [18]. (E) and (F) are modified from [3]. (G) is from D. G. Mackean (http://www.biology-resources.com/drawing-ommatidium-refraction.html)

photo-insensitive membrane (basal membrane). The rhabdomere transduce light into current (LIC), while the basal membrane incorporates different species of voltage-gated K^+ channels, which help to convert LIC into a well-defined voltage response. Rhabdomere (cross-section shown in Fig. 1F) consist of 30,000 finger-like protrusions (microvilli) into the central space. Each microvillus in a rhabdomere is believed to act independently as a phototransduction unit, capturing photons and transducing light energy to a current, which is then used to charge the plasma membrane to generate a voltage response (Fig. 1G).

3 The Model of Photoreceptor

3.1 Photoreceptor Model Structure

The proposed photoreceptor model can be decomposed to several modules, as shown in Fig. 2. The first module (Fig. 2A) corresponds to a random photon capture model, which accounts for the fact that the number of photons absorbed by each microvillus varies across the rhabdomere. The input to this module is a 1 ms light impulse and the output represents the number of photons absorbed by each microvillus. To prevent lateral interactions between microvilli and to keep the integration of LIC linear, the light input was given the maximum effective brightness of 1,000 absorbed photons (1,000,000 photons/s). For this brief stimulation, all photons are assumed to be absorbed at the same time instant. The randomness of photon capture is based on Poisson statistics [4]. It is important to note that $LIC/photon$ (average light induced current per photon) produced in an individual microvillus changes with the number of photons it absorbs. Consequently, it is crucial to have a random photon capture model to produce the light input for each microvillus.

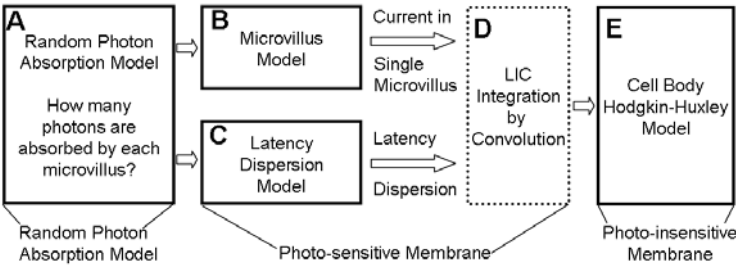

Fig. 2. Schematic structure of our model for impulse light response of *Drosophila* photoreceptor. (A) Random photon absorption model. (B) Deterministic model for phototransduction cascade. (C) Stochastic model for latency dispersion. (D) LIC integration by convolution to produce macroscopic current. (E) Hodgkin-Huxley model for the cell body.

Similar to the anatomical division of the photoreceptor membrane, the processing of light stimuli is performed in two stages. The first processing stage, implemented in modules in Fig. 2B, C, and D, produces the macroscopic LIC

from rhabdomere (photo-sensitive membrane). These signals then drive the second processing stage, a model of the photo-insensitive membrane implemented in Fig. 2E, which accounts for the dynamics of the known voltage-gated ion-channels on the cell body. The processing within a rhabdomere is divided into two parts. The first part (Fig. 2B) is a deterministic model for biochemical reactions of phototransduction cascade within a single microvillus, based on coupled differential equations. The second part (Fig. 2C) is a latency dispersion model that accounts for variations in signal transduction between different microvilli. The latency distribution is obtained through stochastic simulation (Gillespie algorithm) of the phototransduction model. The macroscopic current injected to the cell body is obtained from integration of LIC produced in all microvilli. Under our linear current integration assumption, the integration is produced by convolving the basic current bump (generated by deterministic phototransduction model) with the latency dispersion (Fig. 2D)[19,5].

3.2 Random Photon Absorbtion Model

The random photon absorbtion model is characterized in terms of the following parameters: N_{micro}: the number of microvilli in the whole rhabdomere; N_m: the number of activated microvilli; N_{photon}: the number of photons for the light impulse; $N_p(m_j)$: the number of photons captured by each activated microvillus m_j, $m_j = 1, 2, \ldots, N_m$; λ_M: The average number of light quanta absorbed per microvillus; f_x: the fractions of microvilli that absorb $x = 0, 1, 2 \ldots$ light quanta; f_e: the fraction of microvilli that escape photo-activation; f_a: the fraction of light activated microvilli; λ_p: the average number of photons absorbed by each activated microvillus; $p(k)$: the selection possibility to absorb k photons for each microvillus; k_m: the maximum number of photons each microvillus could absorb; $q(k)$: the accumulation photon selection probability.

The calculation contains two steps. First, N_m is calculated iteratively.

1. Initialization. N_{photon} ($N_{photon} < 1000$), $N_{micro} = 30{,}000$, $N_m = N_{micro}$ (N_m is initially set to N_{micro}, assuming all microvilli are activated).
2. Calculate $\lambda_M = \frac{N_{photon}}{N_m}$.
3. Assuming that f_x follow a Poisson distribution: $f_x = \frac{e^{-\lambda_M} * {\lambda_M}^x}{x!}$. Therefore, $f_e = e^{-\lambda_M}$ and $f_a = 1 - e^{-\lambda_M}$.
4. Update N_m and return to 2 until N_m converged (the termination criteria is heuristic, here, $N_m(i+1) - N_m(i) < 10$, i is the index of current iteration loop).

Then $N_p(m_j)$ is determined based on Poisson distributed roulette rule.

1. Compute λ_p as $\lambda_p = \frac{N_{photon}}{N_m}$.
2. The probability that an activated microvillus m_j can absorb k photons, assuming Poisson distribution, is given by $p(k) = \frac{e^{-\lambda_p} * {\lambda_p}^k}{k!}$. Here, because $N_{photon} \ll N_{micro}$, we assume that $p(k) = 0$ if $k > k_m$, where $k_m = 10 * round(\lambda_p + 1)$ ($round(x)$ obtains the nearest integer of x).

3. Compute $q(k) = \frac{\sum_{j=1}^{k} p(j)}{\sum_{j=1}^{km} p(j)}$, generate a random number r, if $q(k) < r < q(k+1)$, $N_p(m_j) = k$.

Fig. 3 shows simulation results of random photon absorbtion model for a light impulse that contains 600 photons. The number in the x-axis is the number of 'activated microvilli', which is quoted because some of the 'activated microvilli' might absorb 0 photons, meaning failures. The y-axis is the number of photons absorbed by each microvillus. Then microvilli are grouped into different categories based on the number of photons they absorbed ($C(P_h)$ stores the number of microvilli that absorb P_h photons), as the signal transduction properties ($LIC/photon$) vary with this number ($P_h = 1, 2, \ldots, max(N_p)$).

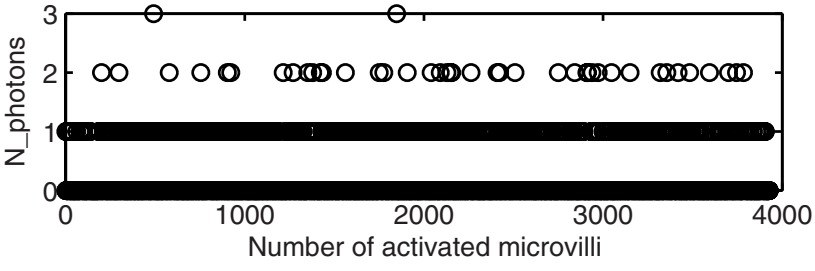

Fig. 3. Simulation of random photon absorbtion model

3.3 Model for Phototransduction Cascade

Molecularbiology of Phototransduction cascade. Although the phototransduction cascade is not fully characterized, it is clear that the photopigment - rhodopsin, thousands of which are densely packed on the microvillar membrane - will change its conformation upon absorption of a photon. This activated rhodopsin (metarhodopsin) then activates a second messenger, G-protein. While bound to metarhodopsin (M), G-protein exchanges inactive guanosine diphosphate (GDP) for active guanosine triphosphate (GTP), which in turn catalyzes phospholipase C (PLC). G-protein coupled PLC cleaves phosphatidyl 4,5-bisphosphate (PIP_2) into two intracellular messengers: inositol trisphosphate (IP_3) and diacylglycerol (DAG). IP_3 is soluble in the cytosol, while DAG is nosoluble and remains bounded to the membrane of microvilli. It is believed that DAG, or its metabolite Polyunsaturated Fatty Acids ($PUFA$), are the excitation messengers to the cation selective ion channels $TRP/TRPL$. The opening of these transduction-channels fluxes in permeable ions, Na^+, Ca^{2+}, Mg^{2+}, generating LIC inside a single microvillus (for review, see [3]). Fig. 4 shows a simplified diagram for *Drosophila* phototransduction cascade.

Regulation of *Drosophila* phototransduction cascade. Molecular, genetic, and physiological studies suggest that at least 20 different gene products are dedicated to the functioning and regulation of this one signaling cascade

in *Drosophila* [3]. There are positive feedback pathways to speed up excitation. TRP channels have a 'all-or-none' excitation property, arising from Ca^{2+} dependent positive feedback to TRP channels. When the first TRP channel opens, the fluxed in Ca^{2+} will excite other TRP channels inside microvillus, triggering many TRP channels to open, untill free intracellular calcium ($[Ca^{2+}]_i$) inside microvillus build up to a level that terminates responses. In addition to excitation, photoreceptor neurons have evolved sophisticated mechanisms for quick termination of LIC (deactivation) to maintain sensitivity. In LIC termination, Ca^{2+} and calmodulin (CAM, Ca^{2+} binding protein, acting as a Ca^{2+} buffer in cytosol) play important roles as negative feedback signals, acting on many target molecules in the phototransduction cascade [2]. Not only can Ca^{2+} provide negative feedback signals to TRP, $TRPL$ channels to facilitate the closure of the channels, but it can also reduce PLC activity, facilitate the binding of arrestin to metarhodopsin (the inactivation process of meta-rhodopsin) [7], *etc.*

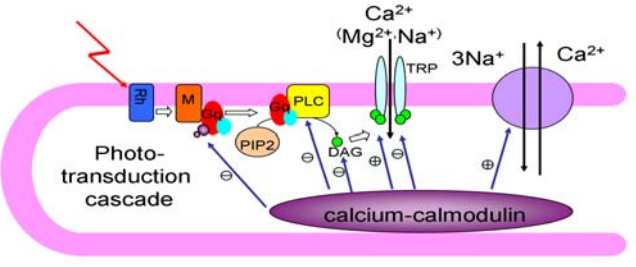

Fig. 4. Phototransduction cascade illustration

3.4 Mathematical Description of Phototransduction Model: Kinetic Equations

The phototransduction cascade model was modified from [15]. The main difference between the models is in Ca^{2+} homeostasis (Eq. 9 to Eq. 12 vs. Eq. 7 and 8 in [15]). The balances, or dynamics, in production and consumption of vital molecules are modeled by nonlinear first-order differential equations. For some of the molecules that are in small numbers, the units are counts of molecules, otherwise, we use concentration (the two are related by the microvillus volume factor, $3 \times 10^{-12}\ \mu l$). To ignore noise effects, all variables are calculated as expectations. In the following equations, the notation X denotes the expected number of molecules, and $X^\star$ will refer to the active state of X, whereas $[X]$ denotes concentration, $[X]_i$ is for intracellular concentration and $[X]_o$ for extracellular concentration. Rates of activation are generically denoted as κ and rates of deactivation denoted as γ.

$$\frac{dM^\star}{dt} = -\gamma_{M^\star} \times (1 + g_{M^\star} f_n) \times \lceil M^\star \rceil. \tag{1}$$

Eq. 1 (vs. Eq. 1 in [15]) is for Metarhodopsin (M). Since all photons are assumed to be effectively absorbed at $t = 0$, there is one-to-one mapping between

number of photons and the value of M. Hence, M is initialized as $M^\star(0) = P_h$. This equation describes the decay of $M^\star$. Compared to [15], we have introduced an additional operator ($\lceil\cdot\rceil$) to avoid negative and non-integer numbers of metarhodopsin. The notation $\lceil M^\star\rceil$ means the smallest integer that is bigger than $M^\star$ if $M^\star > 0$, otherwise $\lceil M^\star\rceil = 0$. The f_n term on the right-hand-side (defined in Eq.8) is negative feedback from $C^\star$ (Ca^{2+} bound CAM). This term is introduced to represent the facilitation of $M^\star$ inactivation by $C^\star$.

$$\frac{dG}{dt} = -\kappa_{G^\star} \times G \times \lceil M^\star\rceil + \gamma_G \times (G_T - G - G^\star) + \kappa_{PLC^\star} \times PLC^\star \times G^\star. \quad (2)$$

$$\frac{dG^\star}{dt} = \kappa_{G^\star} \times G \times \lceil M^\star\rceil - \kappa_{PLC^\star} \times PLC_T \times G^\star. \quad (3)$$

Eqs. 2 and 3 describe activation of G-protein by $M^\star$. There are three states of G-protein, G_qGDP is denoted by G and $G^\star$ represents G_qGTP (active state of G-protein), while the nucleotide-free state of G-protein is calculated as $G_T - G - G^\star$ (G_T is the total number of G-protein inside one microvilli). The first terms in Eq. 2 and in Eq. 3 are modeling exchange from GDP to GTP of G, stimulated by $M^\star$. The seconde term in Eq. 2 is for stabilizing nucleotide-free state G-protein by GDP. The third term in Eq.2 is added on to Eq. 2 in [15] to model the formation of G upon deactivation of $G^\star$ by $GTPase$ activity stimulated by $PLC^\star$. The seconde term in Eq. 3 has two roles in forming the profile of $G^\star$. One role is the conversion of $G^\star$ to PLC complex ($PLC^\star$) by binding to PLC ($\kappa_{PLC^\star} \times (PLC_T - PLC^\star) \times G^\star$, the same with the first term in Eq. 4) and the other role is the conversion of G_qGTP to G_qGDP by $PLC^\star$ ($\kappa_{PLC^\star} \times PLC^\star \times G^\star$, the last term in Eq. 2).

$$\frac{dPLC^\star}{dt} = \kappa_{PLC^\star} \times (PLC_T - PLC^\star) \times G^\star - \gamma_{PLC^\star} \times (1 + g_{PLC^\star} f_n) \times PLC^\star. \quad (4)$$

Eq. 4 represents the dynamics of $PLC^\star$, active PLC complex formed by $G^\star$ and PLC. The last term in Eq. 4 describes deactivation of $PLC^\star$, which was also assumed to be accelerated by negative nonlinear feedback from $C^\star$.

$$\frac{dD^\star}{dt} = \kappa_{D^\star} \times PLC^\star - \gamma_{D^\star} \times (1 + g_{D^\star} f_n) \times D^\star. \quad (5)$$

$PLC^\star$ then cleaves PIP_2 into DAG and IP_3. There is a recycling pathway for PIP_2, but it is much slower than a bump generation ($\sim$ 1,000 times slower, calculated from time constants of the two processes [3]). Hence the dynamics of this recycling is omitted here, leading to a proportional relationship between PIP_2 consumption to number of $PLC^\star$. The response property of second messenger (presumably DAG) could be related directly to $PLC^\star$ and is described by Eq. 5. The interpretation of this equation would be the dynamical balance between the production of DAG from PIP_2 and its degradation through action of DAG-kinase.

$$\frac{dT^\star}{dt} = \kappa_{T^\star} \times (1 + g_{T^\star,p} f_p) \times \left(\frac{D^\star}{K_{D^\star}}\right)^m \times (T_T - T^\star) - \gamma_{T^\star} \times (1 + g_{T^\star,n} f_n) \times T^\star. \quad (6)$$

Eq. 6 describes opening of TRP and $TRPL$ channels (as in [15], we use one equation to describe these two types of channels for simplicity), with $T^\star$ denoting the number of open state channels and T_T the total number of channels, which is conserved inside one microvillus. The precise mechanism of $TRP/TRPL$ activation is not known, but it is likely that 2nd messenger molecules (e.g. DAG) act cooperatively to open one channel. Hence, in Eq.6, the activation rate of $T^\star$ is in proportion to $(\frac{D^\star}{K_{D^\star}})^m$, where m is the cooperativity parameter for DAG molecules and is set to be 4 here).

$$f_p([Ca^{2+}]_i) = \frac{([Ca^{2+}]_i/K_p)^{m_p}}{1 + ([Ca^{2+}]_i/K_p)^{m_p}}. \tag{7}$$

In the dynamics of activation of $TRP/TRPL$ channels, positive feedback signal from Ca^{2+} is included because of the 'all or none' activation properties of these channels. This feedback is formulated as a Hill function of $[Ca^{2+}]_i$ inside microvillus (Eq. 7), where K_p is the dissociation constant, which is $[Ca^{2+}]_i$ that provide half occupancy of Ca^{2+} binding sites for the channels. m_p is the Hill coefficient, describing the cooperativity of Ca^{2+} in exciting the channels. For the acceleration of $TRP/TRPL$ deactivation (refractory transition from open to closed state of the channels), negative feedback is also provided from $C^\star$, the same as the negative feedbacks to other signalling components in the cascade ($M^\star$, $PLC^\star$, $D^\star$, etc). This negative feedback is a sigmoidal shaped function of $C^\star$:

$$f_n([C^\star]) = \frac{([C^\star]/K_n)^{m_n}}{1 + ([C^\star]/K_n)^{m_n}}. \tag{8}$$

where K_n is the dissociation constant and m_n Hill coefficient for $C^\star$. In reality, the affinity of $C^\star$ might vary for different feedback targets, leading to different values of parameters K_n and m_n. However, for simplicity, we look at the whole pool of available $C^\star$ binding sites as the same affinity properties. Feedback strengths are parameterized by g_i. This simplification provides a practical initial approximation, in absence of more complete mechanistic knowledge about the different underlying processes.

The spontaneous activities of all the molecules in the dark, which act as a noise source for the real system, are ignored. Hence, the initial values for the differential equations (Eq. 1 to Eq.6) are set as $G(0) = 50$, $G^\star(0) = 0$, $PLC^\star(0) = 0$, $D^\star(0) = 0$, $T^\star(0) = 0$.

The dynamics of $[Ca^{2+}]_i$ are of particular interests since $[Ca^{2+}]_i$ serves as feedback signal to many targets in the phototransduction cascade. The driving force for $[Ca^{2+}]_i$ is Ca^{2+} entry through $TRP/TRPL$ channels during light response. This Ca^{2+} influx (I_{Ca}) into a microvillus is modeled by Eq. 9:

$$I_{Ca} = P_{Ca} \times I_{T^\star} \times T^\star. \tag{9}$$

$I_{T^\star}$ is the average current fluxed into the cell per TRP channel ($\sim 0.68\, pA/TRP$) and P_{Ca} ($\sim 40\%$) represents the percentage of Ca^{2+} out of the total current influx ($\sim 10\ pA$). At peak response, the Ca^{2+} influx is as high as $10^7\ ions/s$.

Owing to the small volume of a single microvillus, local $[Ca^{2+}]_i$ can rise dramatically. It could peak, for example, at 100 mM during a 20 ms quantum bump, if no other processes were counterbalanced with the influx. In comparison, $[Ca^{2+}]_i$ is about 0.16 μM in the dark state. However, it is important to maintain $[Ca^{2+}]_i$ homeostasis because Ca^{2+} is toxic to the cell in high concentrations.

Apart from Ca^{2+} entry, we model three other processes that modulate $[Ca^{2+}]_i$ dynamics: (i) Ca^{2+} extrusion through Na^+/Ca^{2+} exchanger; (ii) Ca^{2+} buffering by calmodulin; (iii) Ca^{2+} diffusion to the cell body. Na^+/Ca^{2+} exchanger is a conventional transport system with a stoichiometry 3:1, *i.e.* 3 Na^+ ions are exchanged for 1 Ca^{2+} ion. This ratio results in a net charge imbalance, which produces a weakly depolarizing current. The Ca^{2+} current, extruded by the exchanger, is two times the net exchanger current. The net Ca^{2+} influx is obtained by subtracting Ca^{2+} extrusion (through Na^+/Ca^{2+} exchanger) from total Ca^{2+} influx (through TRP channels): $I_{Ca,net} = I_{Ca} - 2 \times I_{NaCa}$, where I_{NaCa} denotes net inward current through Na^+/Ca^{2+} exchanger. The formulation for Na^+/Ca^{2+} exchanger current is adapted from Luo-Rudy model for cardiac cells [8] and is comparable to other models for cardiac myocyte [16]. The model is derived based on thermodynamics of electro-diffusion [9], which assume that the sole source of energy for Ca^{2+} transport is the Na^+ electrochemical gradient.

$$I_{NaCa} = K_{NaCa} \times \frac{1}{K_{m,Na}{}^3 + [Na]_o{}^3} \times \frac{1}{K_{m,Ca} + [Ca]_o} \times \frac{exp(\eta \frac{VF}{RT})[Na]_i{}^3[Ca]_o - exp((\eta-1)\frac{VF}{RT})[Na]_o{}^3[Ca]_i}{1 + d_{NaCa} exp((\eta-1)\frac{VF}{RT})}. \tag{10}$$

where K_{NaCa}, d_{NaCa} are scaling factors, η denotes the (inside) fractional distance into the membrane of the limiting energy barrier. V is the transmembrane potential in volts, ideally this should be from the membrane potential of the cell body. However, as in the simulation, the membrane potential is generated off-line by a separate cell body model, this was approximated by the membrane potential generated by a single Quantum bump. F is the Faraday constant, (96,485 $C \times mol^{-1}$). R is the gas constant (8.314 $J \times K^{-1} \times mol^{-1}$) and T is the absolute temperature, measured in kelvins.

Another Ca^{2+} extruding option might be through the Ca^{2+} uptake by buffering proteins, such as CAM (0.5 mM), which are abundant inside microvillus. The diffusion of buffer molecules over the time scale of interest could be omitted because of the relatively large molecular weight. This binding dynamic was modeled as a first-order process [16]:

$$\frac{dO_c}{dt} = K_U[Ca^{2+}]_i(1 - O_c) - K_R O_c. \tag{11}$$

where, O_c is the buffer occupancy, *i.e.* the fraction of sites already occupied by Ca^{2+} ions, and therefore unavailable for Ca^{2+} binding. $\frac{dO_c}{dt}$ is the temporal rate of change of occupancy of Ca^{2+} binding sites. K_U and K_R are the rate constants for Ca^{2+} uptake and release, respectively. The initial condition for O_c is set, so that $\frac{dO_c}{dt}$ is zero in darkness.

Diffusion between microvillus and somata might also act as a fast free Ca^{2+} shunting. The rate of Ca^{2+} flux from microvillus to somata could be calculated as $\frac{DA}{L}[Ca^{2+}]_i$, whereas $D = 220\ \mu m^2/s$ is diffusivity; $L = 60\ nm$ is length of somata-microvillus membrane neck; $A = 962\ nm^2$ is crossing area of somata-microvillus membrane neck. The rate of Ca^{2+} flux could come out as $10^6\ ions/s$ if $[Ca^{2+}]_i$ were to rise above 10 mM (coinciding with previous published estimations 8 μM-22 mM [14]). Although there are physiological measurements showing that $[Ca^{2+}]_i$ can peak at 200 μM, decaying with characteristic time scale of 100 ms [12], these experiments were done with blowfly in bright condition. Furthermore, $[Ca^{2+}]_i$ may be underestimated by the assumption that all microvilli were stimulated. The amount of diffused Ca^{2+} is comparable to the rate of Ca^{2+} influx at the peak response, so Ca^{2+} diffusion to somata could not be omitted. Ca^{2+} inside microvillus could diffuse $\sim 1\ \mu m$ in 1 ms. Here, the diffusion time is estimated as $2\sqrt{D\Delta t}$: D is the diffusivity, and Δt is the diffusion time interval, which is much less than light response interval. Thus, $[Ca^{2+}]_i$ is assumed to be uniform in the volume of microvillus during light response. Ca^{2+} diffusion is included in the Ca^{2+} dynamics as a regression term, therefore we have our Ca^{2+} dynamics formulated as in Eq. 12:

$$\frac{d[Ca^{2+}]_i}{dt} = \frac{I_{Ca,net}}{2\nu_{Ca}F} - n[B]_i\frac{dO_c}{dt} - K_{Ca}[Ca^{2+}]_i. \tag{12}$$

where $[Ca^{2+}]_i$ dynamic is a balance between net Ca^{2+} influx (first term), Ca^{2+} uptake by Ca^{2+} buffer, calmodulin (seconde term), and Ca^{2+} diffusion (third term). In the second term, n is the number of Ca^{2+} binding sites for calmodulin, here $n = 4$. $[B]_i$ denotes concentration of calmodulin inside the microvillus.

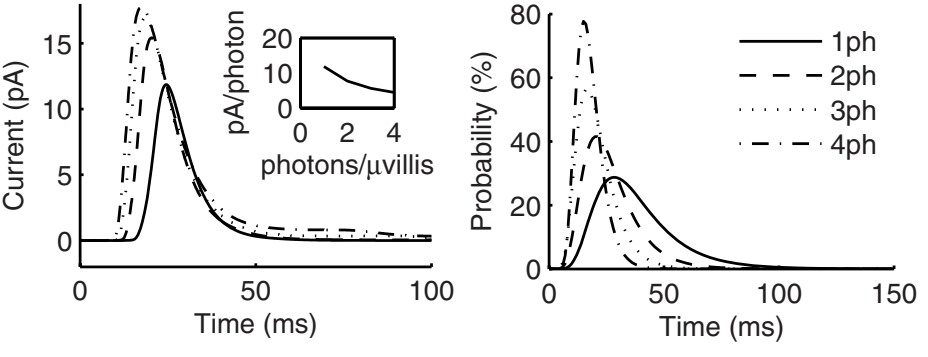

(A) bump shape (B) latencies

Fig. 5. Signal transduction capability at different light level. (A) Basic bump shape when a single microvillus is absorbing 1, 2, 3, 4 photons, the inset shows peak of bump as a function of number of photons absorbed. (B) Average latencies when a single microvillus is absorbing 1, 2, 3, 4 photons. (A) and (B) share the same legend.

Figs. 5A and Fig. 5B, are to show the different signal transduction capability of a single microvillus when it is absorbing different numbers of photons at

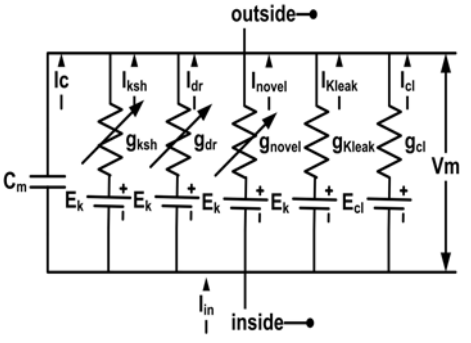

Fig. 6. Electrical circuit of the photoreceptor cell body. Abbreviations: ksh, Shaker channel; dr, delayed rectifier channel; novel, Novel K^+ channel; Kleak, potassium leak conductance; cl, chloride leak conductance.

the same time. It shows that the more photons are absorbed, the less current is produced per photon (the stronger negative feedbacks at brighter light condition; this enables the photoreceptor to effectively use its limited voltage range) and the briefer the latency (the faster are the reactions).

3.5 Model for Latency Dispersion

To overcome the limitations of the deterministic model, which can not describe the variations of signal transduction in different microvilli, we simulated the phototransduction model (Eq. 1 to Eq. 6) stochastically using Gillespie' algorithm. This gives a latency dispersion (time variations in generation of single bumps in different microvilli). For simplicity, we ignore the randomness of the amplitude of different transduction events and assume the randomness only reside in the latencies. The algorithm is from [15]. After simulating phototransduction cascade stochastically for many times, a statistical latency, which is defined as the time for the opening of the first TRP channel, can be obtained. For this, we count the number of emerged bumps in each time bin (histogram of latencies), and use a log-normal function to approximate the statistical latency. Latency distribution is obtained by normalizing the log-normal fit.

3.6 Hodgkin-Huxley Model for Photoreceptor Cell Body

Drosophila photoreceptor express three dominant voltage-sensitive K^+ channels in their photo-insensitive membrane (cell body): shaker and two classes of delayed rectifier that differ in their voltage dependency and rate of inactivation [1]. The resulting activation of voltage-sensitive K^+ channels will extrude K^+ out, and thus oppose light-induced depolarization, driving the membrane toward the dark resting potential.

The model for the photoreceptor cell body was based on Hodgkin-Huxley-formalism (for derivation and validation of the model, refer to [10], supplementary material). The model incorporated Shaker and slow delayed rectifier K^+

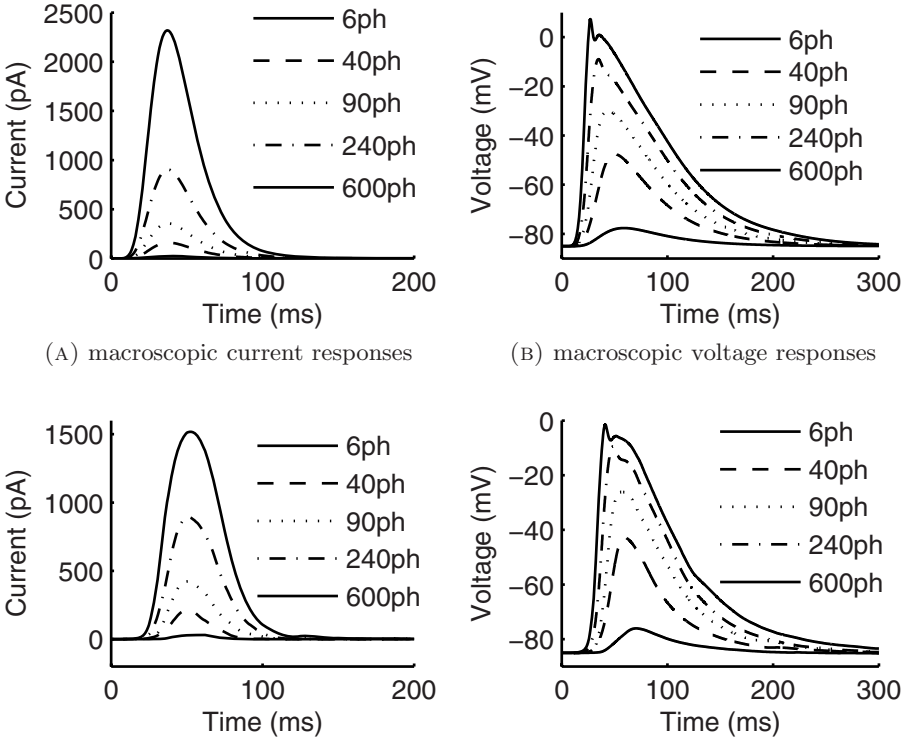

(A) macroscopic current responses

(B) macroscopic voltage responses

(C) macroscopic experimental current responses

(D) experimental current stimulated macroscopic voltage responses

Fig. 7. Simulation results for the model at different light level. (A) Simulated macroscopic current response at light impulse stimuli of 6, 40, 90, 240, 600 photons. (B) Macroscopic voltage responses by the cell body at different level of light impulse stimuli. (C) Experimental macroscopic current responses (patch-clamp data from whole cell recordings) at the same light level shown in Fig. 7A. (D) Voltage response predictions by the model when stimulated by experimental current data.

conductances, in addition to K^+ and Cl^- leak conductances. The voltage-dependent parameters (including time constants and steady-state functions for activation and inactivation of K^+ conductances) were obtained from published data of dark adapted cells [10,1]. Although the properties of delayed rectifier (shab) K^+ channels are regulated by PIP_2 [6], this modulation is much slower than the impulse response of our model. Other photoreceptor membrane properties - *i.e.* the maximum values of the active conductances, resting potential, leak conductances, and membrane capacitance - were estimated from *in vivo* recordings. Though never been measured physiologically, the leak conductances were included to have the right resting potential. It is possible that the leaks could mimic mean inputs from synaptic feedbacks that currently remain uncharacterized. The voltage-dependent properties of the ion channels, the reversal potentials for each

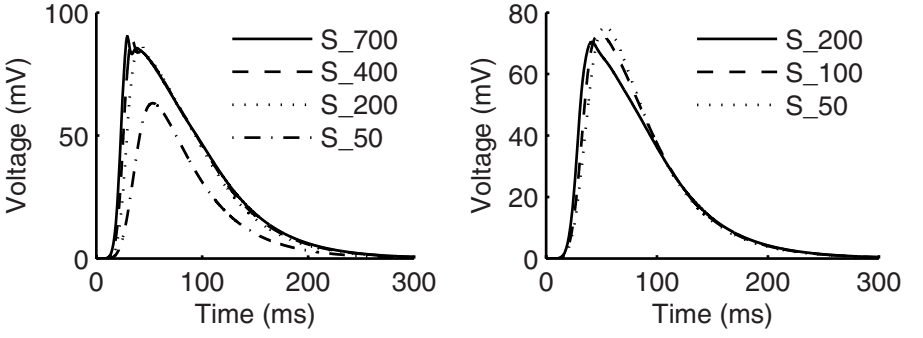

(A) logarithmic scaled voltage responses (B) square root scaled voltage responses

Fig. 8. Scaled voltage responses for comparison. (A) Voltage responses scaled by an logarithmic gain. S_700 depicts the voltage response under 700 photons stimuli. S_400, S_200, S_50 are the 400, 200, 50 photons stimulated voltage responses that are scaled by ln(700)/ln(400), ln(700)/ln(200), ln(700)/ln(50) respectively. (B) Voltage responses scaled by squared root gain under relatively dim light condition (below 200 photons). S_200 shows the voltage response under 200 photons stimuli. S_100, S_50 are the 100, 50 photons stimulated voltage responses that are scaled by sqrt(200)/sqrt(100), sqrt(200)/sqrt(50) respectively.

ion species, and the membrane area were kept fixed within the model. Fig. 6 shows the equivalent electrical circuit for the model, where membrane is modeled as capacitor, the equilibrium potential of different species of ion channels as voltage sources, and different kinds of voltage-gated ion channels as adjustable conductances. Leak channels were modeled as non-adjustable conductances.

The simulated current responses (Fig. 7A) and experimental current (Fig. 7C) responses are very similar in shape. However, the activation and inactivation of the simulated responses are somewhat faster than the experimental ones. This discrepancy might result from the left-shift when approximating the statistical latency with log-normal function, leading to a faster estimate. Nonetheless, the peak of simulated macroscopic current is quite linear with light input (number of photons), about $3 - 4\ pA/photon$, which is in consistent with published data [3]. Whilst the experimental macroscopic current response to 600 photons stimulation appear nonlinear, this compression might be induced by inefficient voltage-clamp control for large currents. The voltage range is almost the same as in Fig. 7B and Fig. 7D, indicating that the cell body model contains the essential nonlinear parts of the cell body. The faster inactivation phase of the estimated voltage response (Fig. 7B) suggests that a log-normal shaped light-induced current might lack a slower boosting component during the inactivation of light response.

Under our simulation, the macroscopic current is quite linear with light intensities, whereas it is the cell body membrane that is highly nonlinear, contributing the most to the compression of voltage responses under relatively bright light

condition. In Fig. 8A, we compared the voltage responses at different light intensities by scaling them with a logarithmic gain. It could be seen that, above 200 photons stimulation, gain scaled voltage responses are quite similar in amplitude. This means that in relatively bright light condition, in logarithmic scale, voltage responses are linear to light intensities. This logarithmic compression under relatively bright light condition help the cell to use efficiently the relatively small voltage range for coding large different light intensities. From our simulation, this compression could be caused mostly by the properties of the voltage gated K^+ conductances. The logarithmic gain control coding is not obtained under relatively dim light condition (under 200 photons/ms), but can be substituted by a square root relationship (Fig. 8B), indicating that cell body membrane could help to shift the gain control mechanism under different light conditions to help using voltage range effectively.

4 Conclusion

We constructed a mathematical model of *Drosophila* R1-R6 photoreceptor to mimic the relationship between voltage outputs and light impulse inputs. The parameters introduced in the model were fixed, if known from electrophysiological experiments, to make physiological sense. Different parts of the models were validated by comparing simulation results with experimental data. The LIC part of the model was validated by comparing the simulation results with *in vitro* patch-clamp data [2] and the cell body model was validated by *in vivo* current injection experiments [10]. Even in this relatively basic form, our model can predict well the waveforms of macroscopic light induced current responses. In the future research, naturalistic light input sequences will be introduced to access the proposed dynamics. The fact that we need to enlarge potassium leak conductance in the current clamp mode to keep voltage responses to light in the right range, indicates there are uncharacterized conductances that facilitate adaptation to varying light levels. Nonetheless, from a practical and systemic point of view, this model can serve as a foundation to a preprocessing module for higher order models of the *Drosophila* visual system that we intend to build due course.

Acknowledgments. We thank A. Pumir for discussion and sharing with Gillespie algorithm, we thank Y. Rudy group and T. Pasi group for discussion of Na^+/Ca^{2+} exchanger model. This work was supported by Biotechnology and Biological Sciences Research Council (BBF0120711 and BBD0019001 to MJ). DC and SAB gratefully acknowledge that this work was supported by the Engineering and Physical Sciences Research Council and the European Research Council. ZS thank The University of Sheffield for Ph.D funding.

References

1. Hardie, R.C.: Voltage-sensitive potassium channels in Drosophila photoreceptors. Journal of Neuroscience 11, 3079–3095 (1991)
2. Hardie, R.C.: Whole-cell recordings of the light induced current in dissociated Drosophila photoreceptors: Evidence for feedback by calcium permeating the light-sensitive channels. Proceedings: Biological Sciences 245, 203–210 (1991)

3. Hardie, R.C., Postma, M.: Phototransduction in microvillar photoreceptors of Drosophila and other invertebrates. The Senses: A Comprehensive Reference 1, 77–130 (2008)
4. Hochstrate, P., Hamdorf, K.: Microvillar components of light adaptation in blowflies. Journal of General Physiology 95, 891–910 (1990)
5. Juusola, M., Hardie, R.C.: Light adaptation in drosophila photoreceptors: I. response dynamics and signaling efficiency at 25 °c. Journal of General Physiology 117, 3–25 (2001)
6. Krause, Y., Krause, S., Huang, J., Liu, C.-H., Hardie, R.C., Weckstrőm, M.: Light-dependent modulation of shab channels via phosphoinositide depletion in Drosophila photoreceptors. Neuron. 59, 596–607 (2008)
7. Liu, C.H., Satoh, A.K., Postma, M., Huang, J., Ready, D.F., Hardie, R.C.: ca^{2+} dependent metarhodopsin inactivation mediated by calmodulin and ninac myosin iii. Neuron. 59, 778–789 (2008)
8. Luo, C.H., Rudy, Y.: A dynamic model of the cardiac ventricular action potential: I. simulations of ionic currents and concentration changes. Circulation Research 74, 1071–1096 (1994)
9. Mullins, L.J.: A mechanism for na^{+}/ca^{2+} transport. Journal of General Physiology 70, 681–695 (1977)
10. J.E. Niven, M. Vähäsőyrinki, M. Kauranen, R.C. Hardie, M. Juusola, and M. Weckstrőm. The contribution of shaker k^{+} channels to the information capacity of *Drosophila* photoreceptors. Nature 6923, 630–634 (2003)
11. Oberwinkler, J.C.: Calcium influx, diffusion and extrusion in fly photoreceptor cells. PhD thesis, University of Groningen (2000)
12. Oberwinkler, J.C., Stavenga, D.G.: Light dependence of calcium and membrane potential measured in blowfly photoreceptors in vivo. Journal of General Physiology 112, 113–124 (1998)
13. Peretz, A., Abitbol, I., Sobko, A., Wu, C.F., Attali, B.: A ca^{2+}/calmodulin-dependent protein kinase modulates Drosophila photoreceptor k^{+} currents: A role in shaping the photoreceptor potential. Journal of Neuroscience 18, 9153–9162 (1998)
14. Postma, M., Oberwinkler, J.C., Stavenga, D.G.: Does ca^{2+} reach millimolar concentrations after single photon absorption in Drosophila photoreceptor microvilli? Biophys. J. 77, 1811–1823 (1999)
15. Pumir, A., Graves, J., Ranganathan, R., Shraiman, B.I.: Systems analysis of the single photon response in invertebrate photoreceptors. Proc. Natl. Acad. Sci. U.S.A 105, 10354–10359 (2008)
16. Rasmusson, R.L., Clark, J.W., Giles, W.R., Robinson, K., Clark, R.B., Shibata, E.F., Campbell, D.L.: A mathematical model of electrophysiological activity in a bullfrog atrial cell. American Journal of Physiology - Heart and Circulatory Physiology 259, 370–389 (1990)
17. van Hateren, J.H., Snippe, H.P.: Phototransduction in primate cones and blowfly photoreceptors: Different mechanisms, different algorithms, similar response. J. Comp. Physiol. A Neuroethol. Sens. Neural. Behav. Physiol. 192, 187–197 (2006)
18. Wolff, T., Ready, D.F.: The Development of Drosophila melanogaster. Cold Spring Harbor Laboratory Press, Plainview (1993)
19. Wong, F., Knight, B.W., Dodge, F.A.: Dispersion of latencies in photoreceptors of limulus and the adapting-bump model. Jounal of General Physiology 76, 517–537 (1980)